JOURNAL OF MORPHOLOGY 241:115–126 (1999)

Skull Allometry in the Marine Toad, *Bufo marinus*

JAMES M. BIRCH*
Department of Biological Sciences, Northern Arizona University, Flagstaff, Arizona

ABSTRACT Scaling predictions pioneered by A.V. Hill state that isometric changes in kinematics result from isometric changes in size. These predictions have been difficult to support because few animals display truly isometric growth. An exception to this rule is said to be the toads in the genus *Bufo*, which can grow over three orders of magnitude. To determine whether skull shape increases isometrically, I used linear measurements and geometric morphometrics to quantify shape variation in a size series of 69 skulls from the marine toad, *B. marinus*. Toads ranged in body mass from 1.8 gm to a calculated 1,558.9 gm. Of all linear measurements (S/V length, skull width, skull length, levator mass, depressor mass, adductor foramen area), only the area of the adductor foramen increased faster than body mass; the remaining variables increased more slowly. In addition, modeling the lower jaw as a lever-arm system showed that the lengths of the closing in- and out-levers scaled isometrically with body mass despite the fact that the skull itself is changing allometrically. Geometric morphometrics discerned areas of greatest variability with increasing body mass at the rear of the skull in the area of the squamosal bone and the adductor foramen. This increase in area of the adductor foramen may allow more muscle to move the relatively greater mass of the lower jaw in larger toads, although adductor mass scales with body mass. If *B. marinus* feeds in a similar manner to other *Bufo*, these results imply that morphological allometry may still result in kinematic isometry. J. Morphol. 241:115–126, 1999.

KEY WORDS: Allometry; morphometrics; scaling; *Bufo*

The tetrapod skull performs functions as varied as protecting the brain to displaying secondary sexual characteristics to acquiring food. Prey acquisition and food processing are particularly important to an animal's survival and reproduction. These behaviors depend on the skull maintaining some sort of functional equivalence throughout ontogeny.

Growth of the skull may constrain feeding behavior because of the different scaling rates of lengths, surface areas, and volumes (Emerson and Bramble, '93). These behavioral changes have been difficult to predict, but A.V. Hill ('50) provided a starting point by describing a null hypothesis that relates isometric size changes and movement. Hill's model predicts that, in geometrically similar animals, the time to perform a movement will be directly proportional to an organism's linear measurements, resulting in constant movement velocities. Confounding these kinematic predictions is the fact that as animals enlarge, the number of muscle sarcomeres in series increases, which increases the maximum shortening velocity of the muscle. Therefore, for movement velocities to remain the same as size increases in geometrically similar animals, the intrinsic rate of muscle shortening must decrease.

These behavioral predictions require animals to increase isometrically (i.e., geometrically) in size as they grow. Although geometric similarity may be present at a gross level (e.g., see Hill ['50] comparing body shapes among cetaceans), upon closer examination geometric similarity is rarely observed in animals due to the structural constraints of morphology (McMahon, '73) or functional

Contract grant sponsor: NSF; Contract grant number: IBN98–09942.

*Correspondence to: James M. Birch, Department of Integrative Biology, University of California, Berkeley, CA 94720-3140.

constraints of behavior (Haldane, '56; Vogel, '88; McGowan, '94).

There have been few studies that describe intraspecific variation in anuran skull shape as body size increases. Instead, work on the skull of anurans has focused on the variation in skull structure among species (e.g., Pusey, '43; Trueb, '66, '68), on patterns of ossification through metamorphosis (Trueb, '85; Wiens, '89), or models predicting skull dimensions based on diet (Emerson, '85). I have undertaken a study of the marine toad, *Bufo marinus,* to determine if this species enlarges isometrically as it grows, and thus if it would be a good candidate for meeting the assumptions and testing the predictions in Hill's model. I chose *B. marinus* because this species 1) has a robust skull that can withstand cleaning with dermestid beetles, 2) has a stereotyped feeding behavior so that function is easily quantifiable (Nishkawa and Gans, '96), and, most importantly, 3) grows over three orders of magnitude. In addition, a preliminary study of a related species, the Colorado river toad *B. alvarius,* has shown that the snout/vent length, skull length, skull width, eye diameter, and narial width all increased as $(\text{body mass})^{0.33}$ (O'Reilly et al., '93), alluding to isometric changes through ontogeny.

Much of the past work in scaling and allometry has used linear measures to determine how shape changes as organisms enlarge (e.g., fishes, Fink ['93]; amphibians, Emerson ['85]; birds, Norberg ['81]; mammals, Norberg and Rayner ['87]). However, this approach overlooks covariation among different parts of the skull during growth (Zelditch et al., '92; Zelditch and Fink, '95). To quantify covariation among different parts of the skull, I used geometric morphometrics to describe how shape changes with skull size. This method models the skull as a constellation of landmarks and describes shape between small and large animals using the covariation among landmarks to identify specific regions of shape change.

The first goal of this project was to determine if the skull of *Bufo marinus* increases isometrically as it grows. Changes of linear measurements with increasing size can be compared to predicted isometric changes. If allometry exists, methods of geometric morphometrics can help identify areas responsible for these allometric changes. A second goal was to examine how the lower jaw and its closing lever-arms change as toads enlarge. Ratios of these lever-arms can provide information on the relative forces and velocities of jaw closing, which may have implications on feeding kinematics in these animals.

MATERIALS AND METHODS

I obtained 69 *Bufo marinus* skulls from animals purchased through the pet trade. This sample consisted of 43 animals purchased specifically for this study, as well as 26 skulls from animals used in an earlier feeding experiment.

From the 43 live animals, I measured body mass, snout/vent length, and the masses of the jaw adductor and abductor muscles. These animals were then killed and the skulls cleaned of flesh using dermestid beetles. Skull measurements were collected using digital calipers to the nearest 0.1 mm and included skull length (the distance from the occipital condyles to the tip of the nasal bone), maximum skull width (measured at the posterior maxilla), squamosal width (measured at the junction of the ventral and anterior/posterior squamosal rami), and the length, in-lever and out-levers of the lower jaw (Fig. 1A,B). The closing in-lever was defined as the distance from the insertion of the jaw adductors to the mandible/quadrate articulation. The closing out-lever was defined as the distance from the jaw tip to the point of articulation with the quadrate.

There were no whole-animal data on the 26 remaining skulls, so I calculated their body mass by generating a regression equation from the 43 live animals, relating maximum skull width to body mass. I then used maximum skull width of these 26 skulls to predict each animal's body mass. These skulls had the same linear measurements taken as the 43 live animals.

All skulls were photographed in dorsal, lateral, and ventral view. On each photograph I digitized homologous landmarks (only one half of the skull in dorsal and ventral views) located at the intersections of sutures or the points of maximum or minimum curvature of bones (Fig. 1A,C,D; Appendix). The dispersion of landmarks permitted description of shape changes over the entire form in each view. Also, from ventral view photographs I measured the area of the adductor foramen using NIH Image (v. 1.61).

The lower jaw was regressed against body mass to test for allometry at a gross level. I then modeled the lower jaw as a simple lever

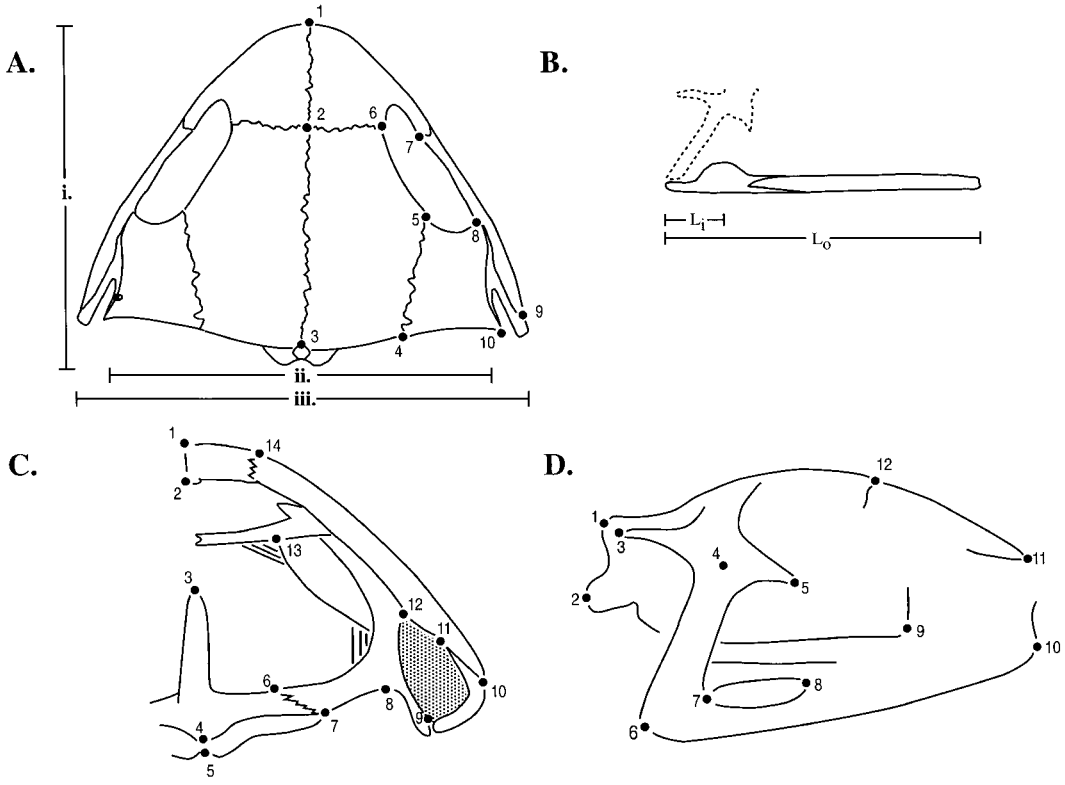

Fig. 1. Landmark locations (described in the Appendix) and traditional measurements taken from *Bufo marinus* skulls. **A**: Dorsal view with [i]) skull length, [ii]) squamosal width, and [iii]) maximum width labeled. **B**: Lower jaw with outline of squamosal/quadrate complex, showing in-lever (L_i) and out-lever (L_o) distances. **C**: Ventral view with adductor foramen shaded. **D**: Right lateral view.

system similar to the methods of Emerson ('85) and Richard and Wainwright ('95). Emerson's ('85) model predicts that closing velocity would be maximized by a high L_o/L_i ratio, whereas closing force would be maximized by a high L_i/L_o ratio, all other things being equal. I regressed L_i against L_o as well as their ratio against log(mass) to determine if jaw lengths were changing in a predictable way as size increases. Although this approach does not take into account the effective lever-arm length of the lower jaw (which changes during mouth opening and closing), or possible changes in muscle force production, and thus cannot predict absolute velocity or force production, I felt the ratio of lever arms would be a good proxy for the relative maximum forces and velocities the lower jaw may experience.

All length, area, and mass measurements were $\log_{10}$ transformed and regressed against body mass using reduced major axis regression. Reduced major axis is preferred over least-squares regression when neither variable is "dependent" or "independent" (Pennycuick, '92; Sokal and Rohlf, '95), although the differences between RMA and simple linear regression were quite small.

Shape analysis

To analyze shape changes that occur with size changes, I used the method of the thin-plate spline decomposed by its relative warps (Bookstein, '91; Rohlf, '93). Bookstein ('91) gives a technical explanation of the statistical methodologies employed during relative warp analysis and the use of the thin-plate spline. Several articles provide less technical explanations of the application of warp analysis (Zelditch et al., '92; Rohlf, '93; Swiderski, '94), so I provide a summary of the methodology used here.

Relative warp analysis is basically a principal coordinate analysis of a Procrustes

similarity matrix. A Procrustes similarity matrix is formed by optimizing the goodness of fit between landmark configurations. There are many ways of optimizing the goodness of fit between two forms (see Chapman, '90), but generally, a similarity coefficient is calculated by superimposing one form over another and "jiggling" landmarks of each form to minimize the distance between as many landmarks as possible. This coefficient is usually calculated as the sum of the squared differences in the coordinates of the two specimens (Rohlf, '90). The coefficients generated from comparisons of many specimens to each other, or comparisons to a consensus specimen, are then assembled in a matrix suitable for principal coordinate analysis.

A principal coordinate analysis simplifies this similarity matrix by calculating orthogonal axes that maximize the amount of explained variation among individuals (Marcus, '90; Reyment and Jöreskog, '93). Components from the principal coordinate analysis are called the relative warps (Bookstein, '91). The first relative warp explains the greatest variability in the scatter-plot of specimens when specimens are plotted by their principal coordinate scores. The second relative warp is orthogonal to the first and explains the next greatest amount of variation, and so on.

The differences discovered through principal coordinate analysis are then depicted by the thin-plate spline. In woodworking, a spline is a narrow, flat piece of wood that fits into a groove or slot in order to join two larger pieces. In an analogous fashion, two forms under comparison can be joined by a mathematical "spline." Certain properties of this spline allow description of shape change at and between landmarks (Bookstein, '91).

The deformation of this spline can be subdivided into two types of change: a uniform and a nonuniform component. The uniform component represents shearing or dilation of an overlaid grid so that parallelograms remain parallelograms after the transformation. Uniform changes are not necessarily due to size, as size was standardized during the Procrustes superposition, but rather the uniform component represents shape change that is identical over the entire form.

The nonuniform component represents differences that are not the same everywhere on the form. Movement of landmarks can change independently of each other, and subdivisions of the nonuniform component of shape change describe changes from large scale (distant landmarks) down to small scale (near landmarks). Subdivisions of the nonuniform component into orthogonal components result in orthogonal axes of variation called the relative warps. Uniform and nonuniform shape changes are two distinct subspaces that, taken together, constitute the full vector space of shape change (Bookstein, '91). In this study, I describe the uniform component and the first three relative warps, since I concentrate on the major components of shape change over a size range.

Uniform and nonuniform changes were estimated using the Thin-Plate Spline (TPS) series of programs developed by J. Rohlf (the latest version can be downloaded from the World Wide Web at http://life.bio.sunysb.edu/morph/). This program computed a mean shape from the 69 individuals, performed a Procrustes and principal coordinate analysis, then depicted the results via the thin-plate spline. The TPS-RW program also allows the setting of a parameter (alpha) that weights shape change at different scales. For example, when alpha = 0, all warps are weighted equally, when there is no a priori reason to expect variation at a particular scale. When alpha = 1, large-scale changes are weighted more heavily than small-scale changes, as would be expected in allometric studies (Rohlf, '93). In this study, I set alpha = 1.

To test for allometry, I regressed the relative warp scores against log(mass). If I found a significant relationship between size and a certain relative warp, I concluded that shape change was not isometric at that level of shape analysis (i.e., that relative warp) but changed allometrically as size increased.

RESULTS

The body mass of toads ranged over almost three orders of magnitude, from 1.8 gm to a calculated 1,558.9 gm. When I regressed squamosal width, snout/vent length, skull length, jaw length, and adductor area against body mass, there was no support for geometric similarity as animals increased in size. Of all the measurements on the skull, only the mass of the levator muscle followed the predictions of isometry. All other measures increased more slowly than predicted by the geometric model, with one exception—the area of the adductor foramen, which increased faster than would be predicted by isometry (Table 1).

TABLE 1. Regression results of linear and mass measurements

	Expected slope	RMA slope	95% C.I.	sem	r^2
Squamosal width	0.33	0.29*	0.287–0.296	0.002	0.996
S/V length	0.33	0.30*	0.293–0.301	0.002	0.997
Skull length	0.33	0.27*	0.263–0.273	0.002	0.994
Jaw length	0.33	0.28*	0.267–0.292	0.006	0.979
Adductor foramen area	0.67	0.84*	0.812–0.868	0.014	0.981
Levator mandibulae mass	1.00	0.97	0.935–1.014	0.019	0.983
Depressor mandibulae mass	1.00	0.84*	0.811–0.873	0.015	0.986

All measurements $\log_{10}$-transformed and regressed against (log)mass.
t-Tests compare reduced major axis (RMA) slopes against expected slope.
*RMA slopes significantly different from expected slope ($P < 0.05$).

The length of the lower jaw also increased more slowly than predicted by isometry (Fig. 2A). Although there was this jaw allometry, the in- and out-levers changed at the same rate (Fig. 2B). When the ratio of in- to out-lever was calculated and regressed against mass, there was appreciable scatter among small animals, but, overall, there was no significant change in this ratio when regressed against this wide range of body masses (Fig. 2C).

Comparing skulls of 1.8 gm toads with those of 1,500 gm toads shows qualitative differences in the size of the orbit and in the width and robustness of the rear of the skull (Fig. 3). When these shape changes are sub-

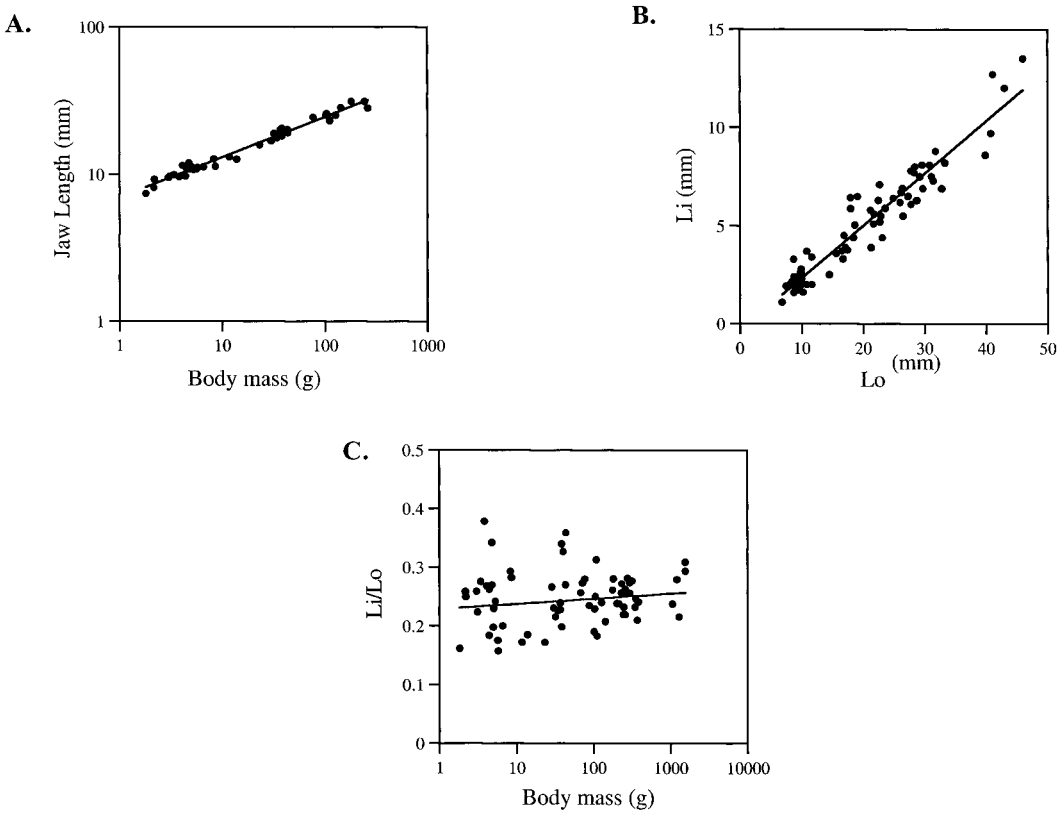

Fig. 2. *Bufo marinus.* Regressions of jaw linear distance against body mass. **A**: Jaw length vs. body mass (slope = 0.28, $r^2 = 0.98$, F = 1894.1, $P < 0.001$). **B**: In-lever vs. out-lever length (slope = 1.07, $r^2 = 0.90$, F = 621.9, $P < 0.001$. **C**: Lever arm ratio vs. body mass (slope = 0.015, $r^2 = 0.02$, F = 1.39, $P = 0.242$).

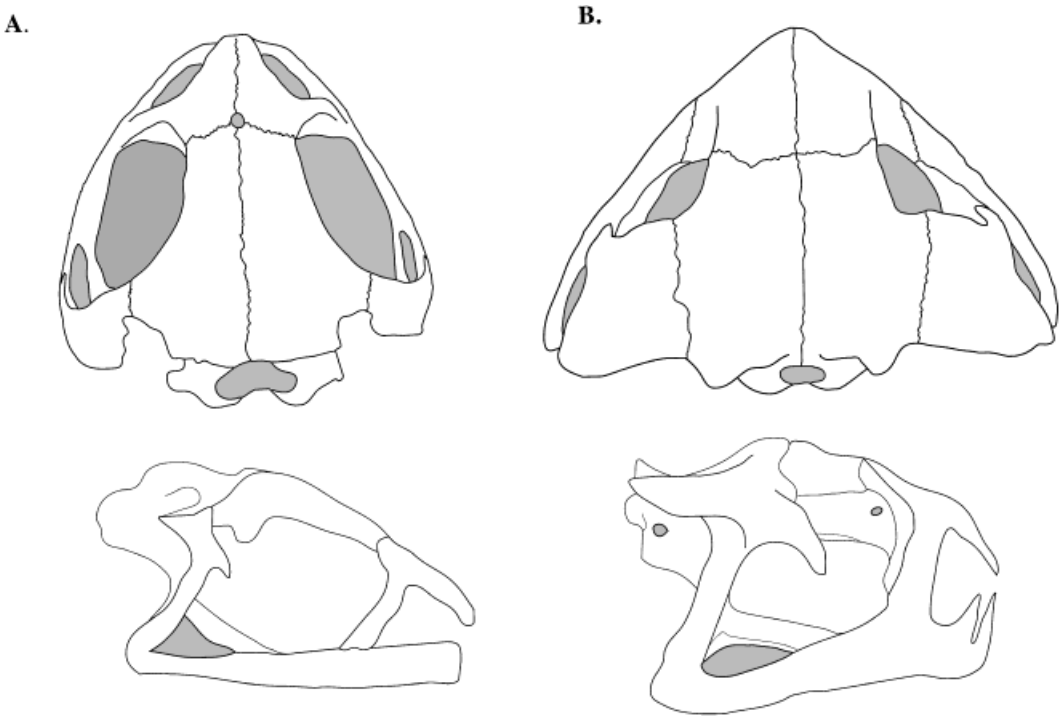

Fig. 3. *Bufo marinus*. Skulls in dorsal and lateral view of (**A**) smallest and (**B**) largest animals scaled to the same skull length. Body mass of animal **A** was 1.8 gm, animal **B** was calculated to be 1,558.9 gm.

divided into uniform and nonuniform components, I found further evidence of allometry.

Uniform shape change

Ventral view

The uniform component is significantly associated with skull growth in both the x and y directions (Fig. 4). Large animals show a significant relationship between x-values of uniform change and body mass ($r^2 = 0.58$, $F = 87.5$, $P < 0.001$), indicating a shearing of all points as animals enlarge, resulting in an anterior shift of the adductor foramen region. Large animals also show a significant relationship between y-values of uniform change and body mass ($r^2 = 0.72$, $F = 161.1$, $P < 0.001$), resulting in a lateral expansion of all points, i.e., larger animals have uniformly wider skulls.

Dorsal view

The pattern of uniform change in dorsal view (Fig. 4) is similar to that seen in ventral view. There is a significant relationship between body mass and changes in both the x- and y-direction of uniform change (x-direction: $r^2 = 0.27$, $F = 23.6$, $P < 0.001$; y-direction: $r^2 = 0.63$, $F = 106.3$, $P < 0.001$). Points distal to the baseline are sheared anteriorly, and there is a uniform lateral expansion of skull width.

Lateral view

There is a significant association between mass and both the uniform expansion of skull height (Fig. 4; y-direction; $r^2 = 0.06$, $F = 4.7$, $P = 0.034$) and the shearing of skull length ($r^2 = 0.49$, $F = 64.4$, $P < 0.001$). This means that small animals have a slight dorsal/ventral compression and an anterior shear of the dorsal points on the skull. Animals with the largest skulls show the opposite change; broadening of the skull dorsoventrally, and a posterior movement of dorsal skull points.

Nonuniform shape change

Ventral view

There was a significant relationship between the first relative warp and mass (Fig.

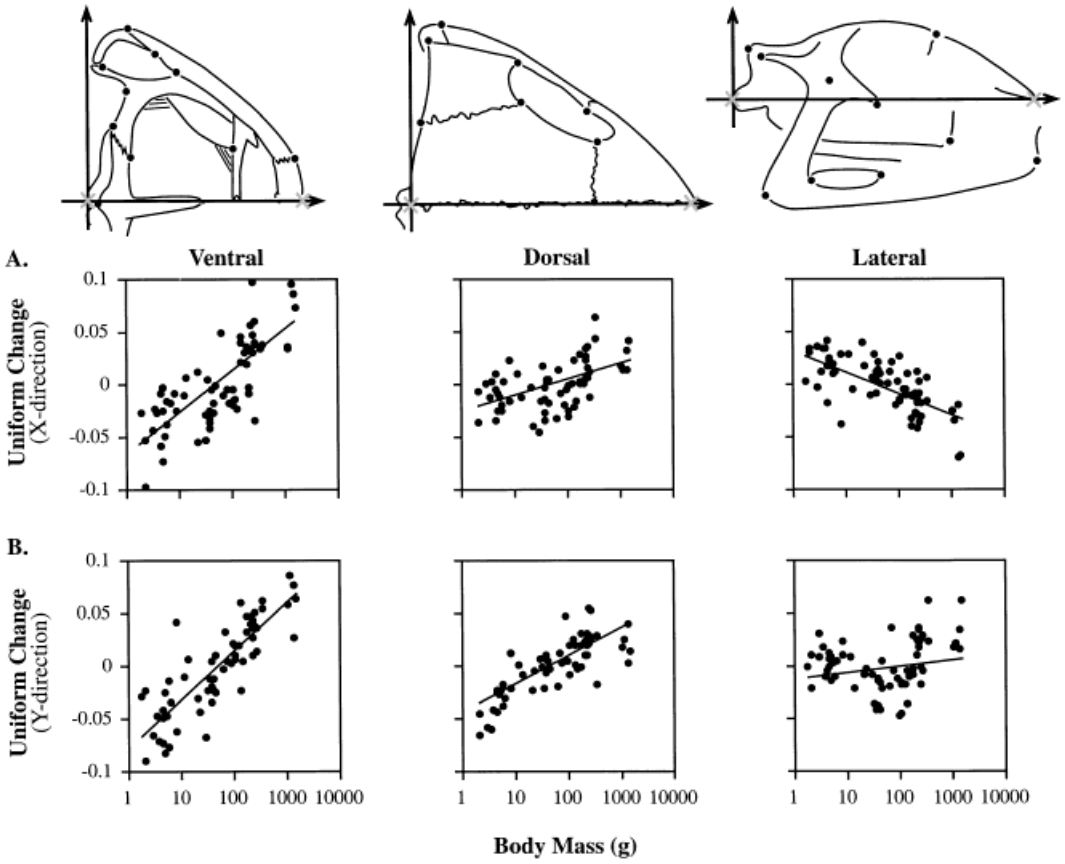

Fig. 4. *Bufo marinus*. Regression of uniform change against size in each view. The baseline for each view has endpoints at coordinates (0,0) and (1,0). Thus, change in the x-direction represents a shearing movement while change in the y-direction represents a uniform expansion or contraction laterally (in ventral and dorsal views) or dorso-ventrally (in lateral views). **A**: x-direction of change. In each view there is a significant relationship between the uniform movement of landmarks in the x-direction and body mass (ventral: $r^2 = 0.57$, $F = 87.5$, $P < 0.001$; dorsal: $r^2 = 0.27$, $F = 23.6$, $P < 0.001$; lateral: $r^2 = 0.49$, $F = 64.4$, $P < 0.001$). In ventral and dorsal view, this relationship manifests itself as an anterior shearing of points in larger animals. In lateral view, larger skulls exhibit a shearing of dorsal points in the posterior direction. **B**: y-direction of change. All three views show a significant relationship between the uniform movement of landmarks in the y-direction, which corresponds to lateral expansion in ventral and dorsal views, and dorso-ventral expansion in lateral view (ventral: $r^2 = 0.72$, $F = 161.1$, $P < 0.001$; dorsal: $r^2 = 0.63$, $F = 106.3$, $P < 0.001$; lateral: $r^2 = 0.06$, $F = 4.7$, $P = 0.034$).

5A; $r^2 = 0.74$; $F = 182.3$; $P < 0.0001$). Large skulls, which have large RW1 scores, show a longitudinal compression, as evidenced by the shortening of the parasphenoid's cultriform process, which results in a relative elongation of the "facial" skull in *Bufo*. Also, large skulls have warp scores that indicate a pronounced allometric enlargement of the adductor foramen (Fig. 5B).

Relative warp 2 is also significantly related to mass (Fig. 5C; $r^2 = 0.11$; $F = 7.7$; $P = 0.007$). As in RW1, there is similar variation in the wing lengths of the parasphenoid and the size of the adductor foramen, but warp 2 also identifies the rostrum as an area of high variability, as seen in the compressed rostrum (landmarks 1, 2, and 14) of small skulls with low scores (Fig. 5D). Relative warp 3 does not show a significant association with mass. In ventral view, warps 1, 2, and 3 combined explain 84.9% of the variation in landmark position.

Dorsal view

There is a significant relationship between the first relative warp and mass in

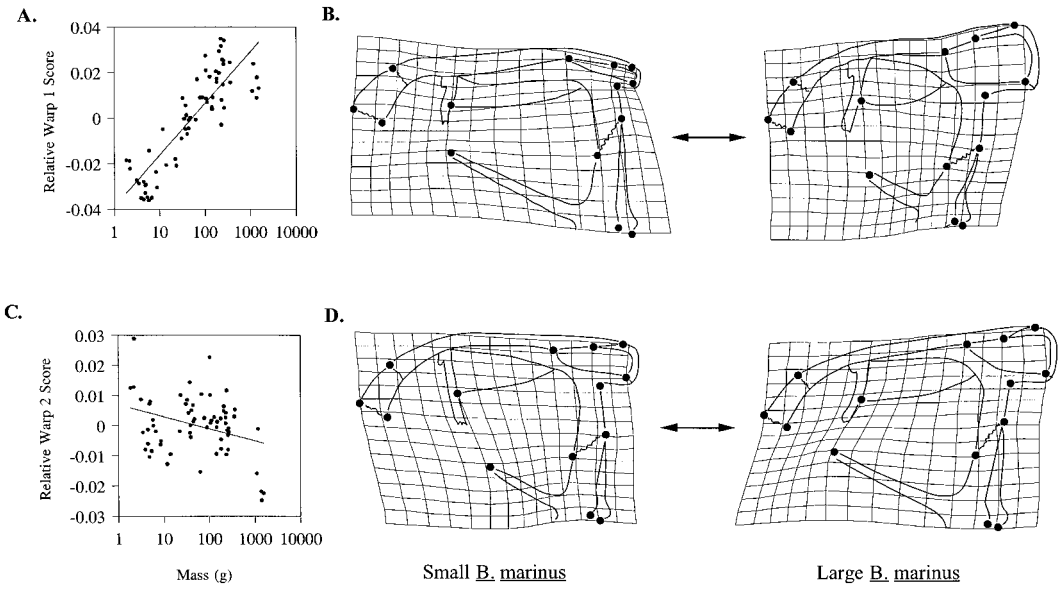

Fig. 5. *Bufo marinus*. The nonuniform shape change in ventral view that is significantly associated with size. **A**: Relative warp 1 vs. body mass ($r^2 = 0.74$, $F = 182.3$, $P < 0.0001$). **B**: The realized shape change along the first relative warp axis. As you move along the first relative warp axis, small skulls "change" to large skulls in the manner depicted by the grids. **C**: Relative warp 2 vs. body mass ($r^2 = 0.11$, $F = 7.7$, $P = 0.007$). **D**: The realized shape change along the second relative warp axis.

dorsal view (Fig. 6A; $r^2 = 0.86$; $F = 373.4$; $P < 0.0001$). The major components of variation are the relative broadening of the skull due to the movement of landmarks 6 and 7 toward the rear of the skull and the increase in the area of the squamosal. As skulls enlarge, there is a decrease in the size of the anterior part of the orbit (the area between landmarks 6 and 7; Fig. 6B). In addition, the squamosal enlarges due to the anterior and posterior edges moving away from each other. Relative warp 2 is also significantly associated with size (Fig. 6C; $r^2 = 0.06$; $F = 4.1$; $P = 0.047$). This warp captures the relative decrease in size of the fronto-parietal bone as animals enlarge, as well as changes associated with maximum skull width (Fig. 6D). Relative warp 3 does not show a significant association with size. In dorsal view, warps 1, 2, and 3 explain 81.5% of the variation in landmark position.

Lateral view

There was a significant relationship between relative warp 1 and mass in lateral view (Fig. 7A; $r^2 = 0.85$; $F = 388.8$; $P < 0.0001$). Large skulls have an expanded squamosal due to the anterior and posterior movements of landmarks 5 and 3, respectively, and a relatively larger ventral ramus, as evidenced by the distance between landmarks 6 and 7. Another interesting result was the generally more robust structure seen in lateral view in larger animals. There was a dorso-ventral expansion as animals enlarge, as well as a diminution of the angle of the squamosal bone relative to the rest of the skull. The squamosal bone of small skulls has a midline that forms an angle of approximately 55° with a line between landmarks 6 and 10, while large skulls have an angle of only 25° (Fig. 7B). In lateral view, relative warps 2 and 3 do not show a significant association with size. Taken together, relative warps 1, 2, and 3 explain 89.6% of the variation in landmark location in lateral view.

DISCUSSION

The goal of this study was to determine how the skull shape of *Bufo marinus* changes with increasing size. The results from both linear measurements and the thin-plate spline analysis demonstrate substantial evidence for allometry; large skulls are not

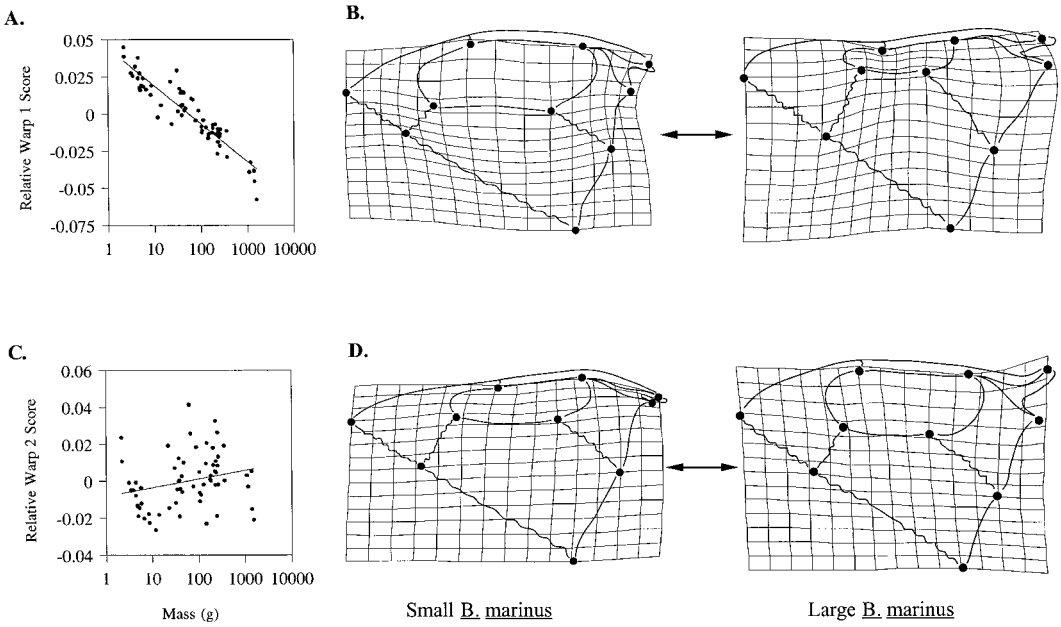

Fig. 6. *Bufo marinus*. The nonuniform shape change in dorsal view significantly associated with size. **A**: Dorsal view; relative warp 1 vs. body mass ($r^2 = 0.86$, $F = 373.4$, $P < 0.0001$). **B**: The realized shape change along the first relative warp axis in dorsal view. As you move along the first relative warp axis, small skulls "change" to large skulls in the manner depicted by the grids. **C**: Relative warp 2 vs. body mass ($r^2 = 0.06$, $F = 4.1$, $P = 0.047$). **D**: The realized shape change along the second relative warp axis.

simply isometric enlargements of small skulls.

It appears that *Bufo marinus* is quite a robust species overall, increasing faster in mass than in linear dimension. Only the mass of the jaw levator increased in proportion to body size, although the adductor foramen area, the opening through which this muscle passes, increased more slowly than predicted by body mass. How could the muscle mass increase in proportion to body mass, yet the opening through which it passes increase more slowly than body mass? This scaling is most likely the result of the levator "fanning out" at its origin in the rear of the orbit. During dissection I noticed relatively more muscle connected at the rear of the orbit in larger animals, yet still narrow-

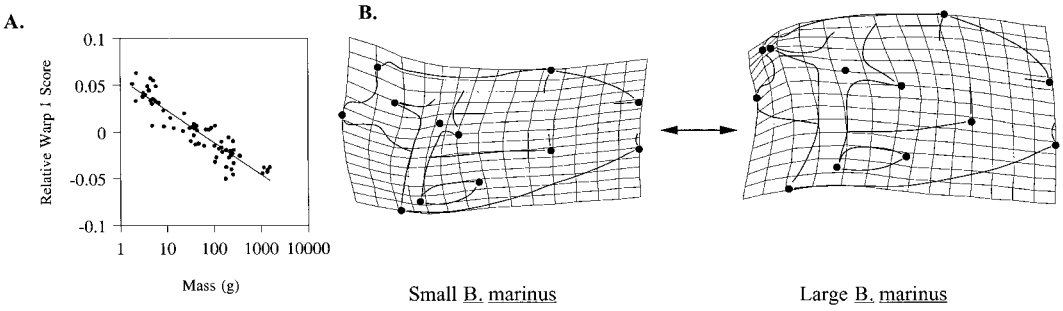

Fig. 7. *Bufo marinus*. The nonuniform shape change in lateral view that is significantly associated with size. **A**: Dorsal view; relative warp 1 vs. body mass ($r^2 = 0.85$, $F = 388.8$, $P < 0.0001$). **B**: The realized shape change along the first relative warp axis in dorsal view. As you move along the first relative warp axis, small skulls "change" to large skulls in the manner depicted by the grids.

ing when passing through the adductor foramen to attach on the lower jaw.

While the jaw length of *Bufo marinus* increases with negative allometry compared to body mass, the closing in-lever and out-lever change at the same rate with respect to each other (Fig. 2B). Emerson ('85) used the ratio of the in- and out-lever as an indicator of relative jaw closing speed and force when comparing the morphology of species that were dietary specialists with those that were dietary generalists. When the ratio of in- to out-lever arms is regressed against body mass, there was no significant relationship (Fig. 2C). This means that, while there was appreciable scatter among small individuals, the lever-arms do not change their relative lengths while toads enlarge. This analysis implies that closing force and closing velocity may increase isometrically with increasing size, although changes in the force production and speed of contraction of the levator and depressor were not measured and may influence this relationship.

Analysis using the thin-plate spline shows similar results in ventral and dorsal views of the skull. Areas of high shape variability are concentrated near the rear of the skull. In ventral view, warps 1 and 2 show that the length of the parasphenoid's cultriform process and the size of the adductor foramen are significantly associated with skull size. In large animals, the skull posterior to the palatine bones (the neural skull sensu Moore, '81) and the adductor foramen enlarge disproportionately (Figs. 5, 6). These changes give the impression of larger skulls having a broader and longitudinally shortened appearance relative to small skulls (Fig. 3). This "broadening" of the rear of the skull is further captured in dorsal view by the decrease in the size of the orbit in large animals and by an increase in size of the dorsal surface of the squamosal bone (Fig. 6).

In lateral view, the most pronounced changes occur in the size and angle of the upper arms of the squamosal (Fig. 7D). Relative to the maxilla, the angle of the dorsal squamosal rami is much flatter in larger animals than in smaller animals. This may provide relatively more area for attachment for both the mm. levator mandibulae and the depressor mandibulae in larger animals. While these osteological results might predict that levator mass should scale with an exponent greater than $M_b^{1.0}$, in fact this muscle did not increase any faster than body mass (Table 1).

There has been little support for Hill's ('50) model on how size affects function in geometrically similar animals because most animals are not similar over a large size range; *Bufo marinus* is no exception to this trend. Alternatively, studies on two different organisms appear to support geometric similarity: the large-mouth bass *(Micropterus salmoides)* and the Colorado River toad *(Bufo alvarius)*. Richard and Wainwright ('95) analyzed feeding behavior in large-mouth bass and found that linear measurements of the head scaled isometrically, as did the linear displacements of the feeding apparatus when regressed against body length. In the Colorado River toad, O'Reilly et al. ('93) showed that linear measurements (including SVL, skull width, skull length, and narial width) scale isometrically with body mass.

Although large-mouth bass and the Colorado River toad display morphological isometry, they differ in their kinematic responses to geometric similarity. Hill ('50) predicted that linear and angular velocities should scale against linear distance with a slope of 1 and 0, respectively. In bass, Wainwright and Richard ('95) found both linear and angular velocities differed significantly from the predicted slopes of 1 and 0, respectively. These kinematic results could not be explained by changing muscle activation patterns as fish grew because size had no effect on any feature of muscle activation (e.g., onset and offset of firing) except the onset time of the adductor mandibulae (Wainwright and Richard, '95). In contrast, the Colorado River toad had duration variables (of mouth opening and closing) that were directly proportional to linear dimensions, indicating isometry (O'Reilly et al., '93). Thus, *Bufo alvarius* comes closest to Hill's ('50) model in terms of both morphology and kinematics.

From unpublished data we have collected, it appears that the kinematic patterns of *Bufo marinus* scale in a way similar to the kinematics of *B. alvarius*. If this is the case, how might allometric size increases result in kinematic isometry? According to Hill's ('50) predictions, isometric changes in shape should result in isometric changes in kinematics. Thus, it appears counterintuitive that as size increases, allometric shape change would result in kinematic isometry. Three lines of reason may explain the observed kinematic isometry.

First, although there is substantial allometry in the skull, the mechanical advantage of the jaw closing muscles remains the same,

regardless of skull size. If the in- and out-lever ratios are maintained throughout ontogeny the jaw will maintain the same opening/closing velocities regardless of animal size, all other things being equal. *Bufo marinus* has in- and out-lever lengths of the lower jaw that scale with a slope that is not statistically different from zero when regressed against body mass. This means that the jaw-lever relationships are maintained throughout ontogeny, although the skull itself changes in both size and shape. If the isometric scaling of these lever arms is constrained by function, I would predict that in frogs that do not use inertia in tongue protraction (e.g., the hydrostatic tongue of *Hemisus marmoratum),* isometry of the in-lever/out-lever ratio should not be necessary and, therefore, may not be found.

Second, functional isometry may result from a change in the per sarcomere rate of shortening (O'Reilly et al., '95). As animals increase in size, the number of sarcomeres in series increases. For movement to remain isometric, the rate of shortening within each sarcomere must decrease. This decrease in rate of shortening is a hypothesis by both Richard and Wainwright ('95) and O'Reilly et al. ('95) to explain the different scaling kinematics they see in bass and toads, respectively. Regardless, the effects of increasing size on the speed of muscle contraction in *Bufo* has not yet been tested.

Third, the results of the shape analysis also suggest that allometric shape change may contribute to the constancy of velocity with increasing size despite incommensurate changes in mass and force. Because mass increases as the cube of a linear distance, but the force a muscle generates increases at only the square of a linear distance, as toads grow larger more muscle must be used to move the lower jaw. One hypothesis for how toads deal with the increasing mass of parts being moved would be to increase the area for attachment of the depressor and levator muscles. This is clearly demonstrated in the amount of shape variation explained along warp 1 in lateral view (Fig. 7B). Larger toads have an expansion of the anterior squamosal ramus, providing additional area for levator muscle attachment. Although there is an increased area for levator attachment, the mass of this muscle is not increasing faster than would be expected from simply growing, so this hypothesis may need reexamination.

Regardless of the relationship between morphological allometry and kinematic isometry, areas of the toad skull most influenced by size are at the rear of the skull, corresponding to areas involved in jaw opening and closing. This variation in skull arrangement must be remembered when trying to account for any functional isometry observed, for the isometry may be the result of morphological allometry.

ACKNOWLEDGMENTS

I thank L. Gray, J. Meyers, and E. Wiltenmuth for helpful discussions during the formulation of this project. K. Nishikawa, J. O'Reilly, and P. Wainwright provided invaluable assistance and helped clarify many issues related to scaling. I thank R. O'Reilly for preparing Figure 1. This work was supported by NSF grant IBN98–09942 to K.C. Nishikawa.

LITERATURE CITED

Bookstein FL. 1991. Morphometric tools for landmark data: geometry and biology. Cambridge: Cambridge University Press. 435 p.

Chapman RE. 1990. Conventional Procrustes approaches. In: Rohlf FJ, Bookstein FL, editors. Special publication 2, proceedings of the Michigan morphometrics workshop. Ann Arbor: University of Michigan Museum of Zoology. p 251–267.

Emerson SB. 1985. Skull shape in frogs—correlations with diet. Herpetologica 41:177–188.

Emerson SB, Bramble DM. 1993. Scaling, allometry, and skull design. In: Hanken J, Hall B, editors: The skull, vol. 3, functional and evolutionary mechanisms. Chicago: University of Chicago Press. p 384–421.

Fink WL. 1993. Revision of the piranha genus *Pygocentrus* (Teleostei, Characiformes). Copeia 1993:665–687.

Haldane JBS. 1956. On being the right size. In: Newman JR, editor. The world of mathematics, vol. 2. New York: Simon & Schuster. p 952–957.

Hill AV. 1950. The dimensions of animals and their muscular dynamics. Sci Prog 38:209–230.

Marcus LF. 1990. Traditional morphometrics. In: Rohlf FJ, Bookstein FL, editors. Special publication 2, proceedings of the Michigan morphometrics workshop. Ann Arbor: University of Michigan Museum of Zoology. p 77–122.

McGowan C. 1994. Diatoms to dinosaurs. The size and scale of living things. Washington D.C.: Island Press. 288 p.

McMahon T. 1973. Size and shape in biology. Science 179:1201–1204.

Moore WJ. 1981. The mammalian skull. Cambridge: Cambridge University Press. 369 p.

Nishikawa KC, Gans C. 1996. Mechanisms of tongue protraction and narial closure in the marine toad *Bufo marinus.* J Exp Biol 199:2511–2529.

Norberg UM. 1981. Allometry of bat wings and legs and comparison with bird wings. Philos Trans R Soc Lond B Biol Sci 292:359–398.

Norberg UM, Rayner JMV. 1987. Ecological morphology and flight in bats (Mammalia: Chiroptera): wing adaptations, flight performance, foraging strategy and echolocation. Philos Trans R Soc Lond B Biol Sci 316:335–427.

O'Reilly JC, Lindstedt SL, Nishikawa KC. 1993. The scaling of feeding kinematics in toads (Anura: Bufonidae). Am Zool 33:147A (583).

O'Reilly JC, Lindstedt SL, Nishikawa KC. 1995. Speed of movement in geometrically similar animals: a test of a prediction made by A.V. Hill. FASEB J 9:A79 (463).
Pennycuick CJ. 1992. Newton rules biology. New York: Oxford University Press. 111 p.
Pusey HK. 1943. On the head of the leiopelmid frog, *Ascaphus truei*. I. The chondrocranium, jaws, arches, and muscles of a partly-grown larva. Q J Mic Sci 84:106–185.
Reyment RA, Jöreskog KG. 1993. Applied factor analysis in the natural sciences. Cambridge: Cambridge University Press. 371 p.
Richard BA, Wainwright PC. 1995. Scaling the feeding mechanisms of largemouth bass *(Micropterus salmoides):* kinematics of prey capture. J Exp Biol 198:419–433.
Rohlf, FJ. 1990. Rotational fit (Procrustes) methods. In: Rohlf FJ, Bookstein FL, editors. Special publication 2, proceedings of the Michigan morphometrics workshop. Ann Arbor: University of Michigan Museum of Zoology. p. 227–236.
Rohlf, FJ. 1993. Relative warp analysis and an example of its application to mosquito wings. In: Marcus LF, Bello E, Garcia-Valdecasas A, editors. Contributions to morphometrics. Madrid, Spain: Monografias del Museo Nacional de Ciencias Naturales. p 131–159
Sokal RR, Rohlf FJ. 1995. Biometry, 3rd ed. New York: W.H. Freeman. 887 p.
Swiderski DL. 1994. Morphological evolution of the scapula in tree squirrels, chipmunks, and ground squirrels (Sciuridae): an analysis using thin-plate splines. Evolution 47:1854–1873.
Trueb L. 1966. Morphology and development of the skull in the frog *Hyla septentrionalis*. Copeia 1966:562–573.
Trueb L. 1968. Cranial osteology of the hylid frog, *Smilisca baudini*. Univ Kan Pub Mus Nat Hist 18: 11–35.
Trueb L. 1985. A summary of osteocranial development in anurans with notes on the sequence of cranial ossification in *Rhinophrynus dorsalis* (Anura: Pipoidea: Rhinophrynidae). S Afr J Sci 81:181–185.
Vogel S. 1988. Life's devices. The physical world of animals and plants. Princeton, NJ: Princeton University Press. 367 p.
Wainwright PC, Richard BA. 1995. Scaling the feeding mechanisms of largemouth bass *(Micropterus salmoides):* motor pattern. J Exp Biol 198:1161–1171.
Wiens JJ. 1989. Ontogeny of the skeleton of *Spea bombifrons* (Anura: Pelobatidae). J Morphol 202:29–51.
Zelditch ML, Fink WL. 1995. Allometry and developmental integration of body growth in a piranha, *Pygocentrus nattereri* (Teleostei: Ostariophysi). J Morphol 223: 341–355.
Zelditch ML, Bookstein FL, Lundrigan BL. 1992. Ontogeny of integrated skull growth in the cotton rat *Sigmodon fulviventer*. Evolution 46:1164–1180.

APPENDIX
Landmarks

Ventral view

1. Tip of upper jaw
2. Junction of the palatine process and premaxilla
3. Tip of cultriform process of the parasphenoid bone
4. Posterior tip of parasphenoid bone along the midline
5. Notch between the occipital condyles
6. Tip of the medial ramus of the pterygoid
7. Tip of the lateral parasphenoid wing
8. Junction of the posterior and medial rami of the pterygoid
9. Anterior junction of the posterior pterygoid ramus and the quadratojugal
10. Posterior tip of maxilla (seen below/around quadratojugal)
11. Junction of the anterior tip of the quadratojugal and the maxilla
12. Anterior point of the adductor foramen at the maxilla-pterygoid junction
13. Junction of the frontal/sphenethmoid and palatine
14. Labial junction of the maxilla and premaxilla

Dorsal view

1. Tip of nasal bones along the midline
2. Junction of the nasal/frontoparietal along midline
3. Junction of the frontoparietals at the foramen magnum
4. Posterior squamosal/frontoparietal junction
5. Anterior squamosal/frontoparietal junction
6. Nasal/frontoparietal junction at the orbit
7. Nasal/maxilla junction
8. Tip of zygomatic ramus of the squamosal
9. Junction of maxilla and ventral ramus of the squamosal
10. Tip of otic ramus of the squamosal

Lateral view

1. Tip of exoccipital process
2. Tip of occipital condyle
3. Tip of otic ramus of the squamosal
4. Center of the ventral ramus of squamosal between landmarks 3 and 5
5. Tip of zygomatic ramus of squamosal
6. Posterior point of quadratojugal
7. Maxilla/squamosal junction
8. Anterior point of the adductor foramen at the maxilla-pterygoid junction
9. Junction of the maxilla and nasal bone
10. Tip of upper jaw
11. Tip of nasal bone
12. Junction of the frontoparietal and nasal